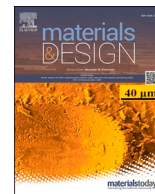


Title	Quasi-direct Cu-Si <sub>3</sub> N <sub>4</sub> bonding using multi-layered active metal deposition for power-module substrate
Author(s)	Tatsumi, Hiroaki; Moon, Seongjae; Takahashi, Makoto et al.
Citation	Materials and Design. 2024, 238, p. 112637
Version Type	VoR
URL	<a href="https://hdl.handle.net/11094/94583">https://hdl.handle.net/11094/94583</a>
rights	This article is licensed under a Creative Commons Attribution 4.0 International License.
Note	

*Osaka University Knowledge Archive : OUKA*

<https://ir.library.osaka-u.ac.jp/>

Osaka University



## Quasi-direct Cu–Si<sub>3</sub>N<sub>4</sub> bonding using multi-layered active metal deposition for power-module substrate

Hiroaki Tatsumi<sup>a,\*</sup>, Seongjae Moon<sup>b</sup>, Makoto Takahashi<sup>a</sup>, Takahiro Kozawa<sup>a</sup>, Eiki Tsushima<sup>b</sup>, Hiroshi Nishikawa<sup>a</sup>

<sup>a</sup> Joining and Welding Research Institute, Osaka University, 11-1 Mihogaoka, Ibaraki, Osaka 567-0047, Japan

<sup>b</sup> FJ Composite Materials Co., LTD., 2-2-3 Kashiwadai Minami, Chitose, Hokkaido 066-0009, Japan

### ARTICLE INFO

#### Keywords:

Silicon nitride  
Ceramic insulating circuit substrate  
Cu–Si<sub>3</sub>N<sub>4</sub> bonding  
Bonding interface

### ABSTRACT

The advancement of power modules demands more reliable insulating circuit substrates. Traditional substrates, comprising Cu and Si<sub>3</sub>N<sub>4</sub>, are produced using active metal brazing (AMB). However, AMB substrates have reliability concerns owing to electrochemical migration and void formation from brazing filler metals. This study introduces a quasi-direct Cu–Si<sub>3</sub>N<sub>4</sub> bonding technique using a Ti/Al bilayer active metal deposition at the bonding interface. A sputtered Ti/Al bilayer was formed on the Si<sub>3</sub>N<sub>4</sub> surface, then heated and pressurized the sputtered Si<sub>3</sub>N<sub>4</sub> substrate with Cu sheets in vacuum to bond each other without voids or delamination. The Ti/Al layers reacted with Si<sub>3</sub>N<sub>4</sub> and Cu, forming a 300 nm intermediate layer. TEM observations show this layer contains segregated Ti–N and Cu–Al phases, with a good lattice match to Si<sub>3</sub>N<sub>4</sub> and Cu–Al. Temperature-cycling tests on the Cu/Si<sub>3</sub>N<sub>4</sub>/Cu substrate revealed delamination caused by increased tensile stress at the periphery of the bonding area due to asymmetrical Cu patterns. This novel quasi-direct Cu–Si<sub>3</sub>N<sub>4</sub> bonding technique addresses issues of electrochemical migration and void formation seen in AMB substrates, offering a reliable bonding interface for power electronic substrates.

### 1. Introduction

In the field of power electronics, where efficient power conversion and control are crucial, advanced power modules are in high demand to improve efficiency, while reducing the size and cost of systems for various applications, including electric vehicles, renewable energies, and industrial motors and generators [1]. The insulating circuit substrates used in these advanced power modules must withstand high voltages [2,3] and accommodate large power capacities during high-temperature cyclic operations [4,5]. Therefore, improving the heat dissipation capability and temperature-cycle operation reliability of these insulating circuit substrates is imperative [6]. An insulating circuit substrate typically comprises a ceramic insulating substrate with Cu sheets bonded on both sides. Common options for the ceramic insulating substrate include Al<sub>2</sub>O<sub>3</sub>, AlN, and Si<sub>3</sub>N<sub>4</sub> [7–9]. Si<sub>3</sub>N<sub>4</sub> is particularly promising as an insulating ceramic material because of its excellent mechanical properties [10,11] for next-generation power modules that require severe temperature cycling. To achieve insulating circuit boards with excellent heat dissipation and high thermal cycling reliability, a

bonding technology to laminate Si<sub>3</sub>N<sub>4</sub> and Cu is essential.

In general, bonding ceramics, especially Si<sub>3</sub>N<sub>4</sub> and metal, is challenging owing to their poor affinities. Active metals such as Ti, Al, and Cr, which tend to form strong bonds with ceramics, have been employed in bonding technologies. The most common process for bonding Si<sub>3</sub>N<sub>4</sub> insulated circuit boards is the active metal brazing (AMB) method [12], which uses active brazing filler metals comprising Ag–Cu–Ti. The resulting product is called an AMB substrate. In this method, a brazing filler metal paste is printed between a Si<sub>3</sub>N<sub>4</sub> substrate and Cu plates, followed by heating in a vacuum atmosphere to obtain brazed joints. However, the tendency for void formation in the brazing layer causes issues with heat dissipation and the bonding reliability of AMB substrates [13,14]. Furthermore, Ag is known to be the element most susceptible to electrochemical migration (ion migration) [15]; therefore, using AMB substrates in high-voltage environments may result in fatal circuit failure owing to the electrochemical migration of Ag at the brazing interface [16].

Diffusion bonding [17] is a direct solid-state bonding technique that does not use (or uses an extremely small amount of) molten materials,

\* Corresponding author.

E-mail address: [tatsumi.jwri@osaka-u.ac.jp](mailto:tatsumi.jwri@osaka-u.ac.jp) (H. Tatsumi).

<https://doi.org/10.1016/j.matdes.2024.112637>

Received 19 October 2023; Received in revised form 6 December 2023; Accepted 3 January 2024

Available online 6 January 2024

0264-1275/© 2024 The Author(s). Published by Elsevier Ltd. This is an open access article under the CC BY license (<http://creativecommons.org/licenses/by/4.0/>).

such as brazing filler metals. Compared with the AMB method, it offers advantages such as ease in suppressing reaction layer formation at the bonding interface, high conductivity owing to the directly bonded interface, and the absence of elements that may cause electrochemical migration. However, this bonding technique has the drawback of requiring high temperatures and extended bonding time to facilitate the diffusion reaction responsible for bonding to eliminate gaps at the bonding interface. Transient liquid-phase (TLP) diffusion bonding is another possible approach for Cu–ceramic bonding. TLP bonding utilizing Cu and oxygen eutectic reactions at 1065 °C, known as the direct bonding copper (DBC) technique, has been widely employed for Cu–Al<sub>2</sub>O<sub>3</sub> and Cu–AlN bonding [18], but not for Cu–Si<sub>3</sub>N<sub>4</sub> owing to their poor affinity. Therefore, direct bonding between Cu and Si<sub>3</sub>N<sub>4</sub> remains a challenge.

To achieve a good bond between Si<sub>3</sub>N<sub>4</sub> and Cu without using active brazing filler metals, two major approaches have been proposed: direct bonding methods involving surface modification and additively manufactured direct bonding methods. As surface modification processes, laser irradiation techniques have been reported for fabricating direct-bonded Si<sub>3</sub>N<sub>4</sub>–Cu interfaces via surface-local thermal decomposition of Si<sub>3</sub>N<sub>4</sub> [19,20]. These processes have shown that the thermally decomposed surface layer, comprising polycrystalline Si derived from Si<sub>3</sub>N<sub>4</sub>, enhances the direct bonding capability of Cu. As an additively manufactured direct bonding method, a sequential atmospheric plasma spray (APS) process involving Cu and Ti powders on Si<sub>3</sub>N<sub>4</sub> was employed to fabricate a Cu/Ti/Si<sub>3</sub>N<sub>4</sub> layered structure [21]. Furthermore, the spark plasma sintering (SPS) method was used to fabricate a nanocrystalline Cu layer on a Si<sub>3</sub>N<sub>4</sub> substrate [22]. These direct bonding techniques are still being explored to optimize the formation of an interface structure with a high affinity for the Si<sub>3</sub>N<sub>4</sub> surface while minimizing gaps at the bonding interface.

To achieve a favorable Cu–Si<sub>3</sub>N<sub>4</sub> interface structure suppressing void formation and Ag-derived electrochemical migration, we propose a quasi-direct Cu–Si<sub>3</sub>N<sub>4</sub> bonding technique using a Ti/Al bilayered active metal deposition on the bonding interface. Initially, a sputtered thin film comprising a Ti/Al bilayer was formed on the Si<sub>3</sub>N<sub>4</sub> surface as the active metal. Subsequently, Cu–Si<sub>3</sub>N<sub>4</sub> bonding was performed by heating and pressurizing in a vacuum atmosphere. Furthermore, this study analyzes the bonding interface using electron microscopy and examines the results of the thermal cycling reliability of an insulated circuit board. This study provides valuable information and contributes to the development of efficient and reliable bonding technologies for power electronics applications.

## 2. Experimental and numerical procedures

A schematic of the bonding procedure is shown in Fig. 1. First, a Ti/Al dual layer was deposited on both sides of a  $\beta$ -Si<sub>3</sub>N<sub>4</sub> substrate using Ar plasma sputtering with a direct current (DC) power source. The dimensions of the Si<sub>3</sub>N<sub>4</sub> substrate were 140 mm × 190 mm × 0.32 mm. These deposition processes were conducted continuously in a sputtering chamber to prevent exposure to air. Subsequently, the Ti/Al-deposited Si<sub>3</sub>N<sub>4</sub> substrate was stacked between the Cu sheets, as shown in Fig. 1 (b). The dimensions of the Cu sheets were 140 mm × 190 mm × 0.3 mm. The stacked Si<sub>3</sub>N<sub>4</sub> substrate and Cu sheets underwent bonding, as shown in Fig. 1(c). After placing the stacked substrate, the chamber was closed, and a vacuum atmosphere of  $1 \times 10^{-3}$  Pa was created. The stacked substrate was gradually subjected to a uniaxial compressive stress of 15 MPa, heated to 950 °C with the heating time of approximately 1 h, and then held for 1 h. Subsequently, the substrate was gradually cooled to room temperature inside the chamber with the cooling time of approximately 4 h, and the uniaxial stress was released. Subsequently, the bonded substrate was chemically etched with copper (II) chloride solution to partially remove the Cu parts to form circuits. Finally, the chemically etched substrates were cut into 28 mm × 28 mm pieces using a diamond wire saw. The schematics and dimensions of the fabricated Cu/Si<sub>3</sub>N<sub>4</sub>/Cu substrate are shown in Fig. 1(d).

The surface morphology of the as-deposited Si<sub>3</sub>N<sub>4</sub> substrate prior to bonding was characterized using scanning electron microscopy (SEM, SU-70, Hitachi High-Tech Corporation, Japan) and energy dispersive X-ray spectroscopy (EDX). The deposited Ti/Al layer structure was characterized via depth analysis using X-ray photoelectron spectroscopy (XPS, PHI 5000 VersaProbe III, Ulvac-PHI Inc., Japan), where Al K $\alpha$  was used as the X-ray source (15 kV), and the area for the analysis was approximately  $\phi$ 100  $\mu$ m. XPS depth analysis was performed by sputtering with Ar ions. The sputtering depth was determined based on the sputtering time, assuming a sputtering rate equivalent to that of SiO<sub>2</sub> (7.08 nm/min). The thickness of each layer was determined using the full width at half maximum.

The cross-sectional microstructure at the bonding interface between Si<sub>3</sub>N<sub>4</sub> and Cu was analyzed via SEM using an Ar-ion beam cross-sectional polisher (SM-09010, JEOL Ltd., Japan). The interfacial crystalline structure was further evaluated using transmission electron microscopy (TEM, JEM-2100F, JEOL Ltd., Japan). TEM samples were prepared using a focused ion beam (FIB, FB-2000A, Hitachi Ltd., Japan).

To investigate the thermal cycling reliability, the fabricated Cu/Si<sub>3</sub>N<sub>4</sub>/Cu substrates were subjected to thermal cycling test (TCT) up to

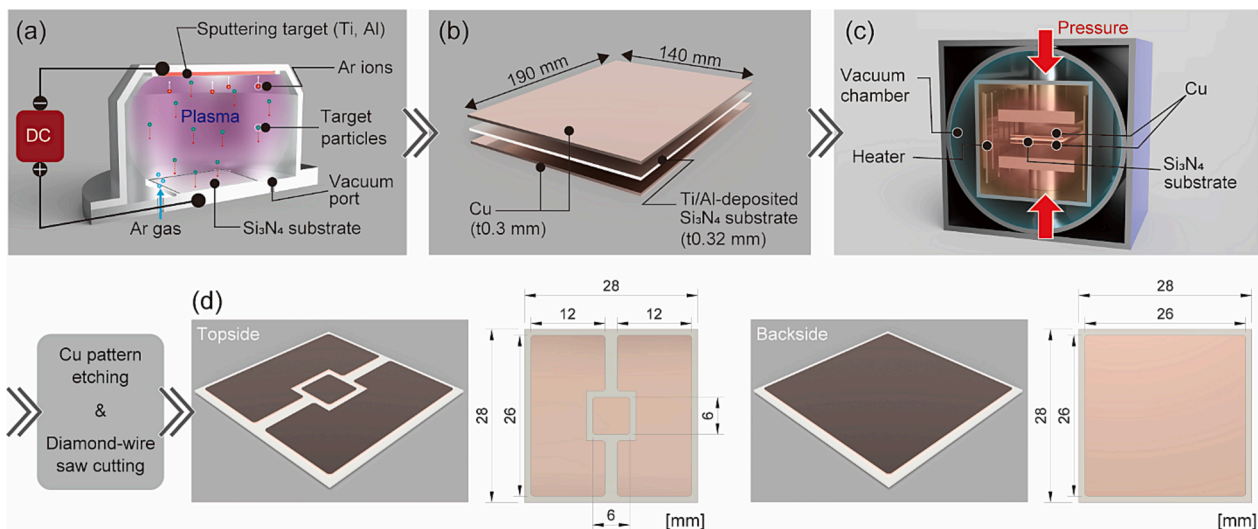


**Fig. 1.** Schematic of the bonding procedure: (a) sputtering deposition process, (b) Cu and Si<sub>3</sub>N<sub>4</sub> substrates, (c) uniaxially pressurized bonding process in a vacuum atmosphere, and (d) schematic of the fabricated Cu/Si<sub>3</sub>N<sub>4</sub>/Cu substrate.

600 cycles between  $-40$  and  $200$  °C with 20 min dwell times using a thermal cycling chamber (TSA-43EL-A, ESPEC Corp., Japan). The total duration of one cycle was 40 min, with heating and cooling completed within 1 min. Nondestructive observations were conducted at temperature cycling steps of 0, 100, 200, 400, and 600 cycles using scanning acoustic tomography (SAT, FS100III, Hitachi Ltd., Japan). The observed images were used to calculate the delamination area ratio using image-editing software.

A mechanical finite element (FE) simulation was performed using the commercial software ANSYS Mechanical 2023 R1 to investigate the stress and strain distributions during TCT. A three-dimensional (3D) FE model was constructed by incorporating a  $\text{Si}_3\text{N}_4$  substrate flanked by Cu layers. The dimensions of the FE model correspond to those shown in Fig. 1(d). Here, a 1/2 model was used for the simulation, considering the symmetry conditions. Ideal contact was assumed between all interfaces. The intermediate layer between Cu and  $\text{Si}_3\text{N}_4$ , as shown in Fig. 3(b), was omitted from the model because it had negligible influence on the resulting stress and strain distributions. Quadratic hexahedral elements were used, and the numbers of nodes and elements in the model were 281,588 and 59,605, respectively. Cu and  $\text{Si}_3\text{N}_4$  were considered as multilinear elastoplastic and linear elastic materials, respectively. The mechanical properties of Cu were treated as temperature dependent, whereas those of  $\text{Si}_3\text{N}_4$  were not. The relevant parameters are listed in Table 1. The stress and strain distributions were calculated for ten steady-state cycles where the temperature oscillated between  $-40$  and  $200$  °C. Thermal stress and strain were generated owing to a mismatch in the coefficient of thermal expansion (CTE) among the constituent materials during temperature variation.

### 3. Results and discussion

#### 3.1. Cu- $\text{Si}_3\text{N}_4$ interface structure

First, the Ti/Al layer deposited on the  $\text{Si}_3\text{N}_4$  substrate before the bonding process was evaluated using SEM and XPS depth analysis. The SEM image of the as-deposited  $\text{Si}_3\text{N}_4$  substrate surface in Fig. 2(a-1) shows a typical uneven surface morphology [26] owing to irregularly shaped raw  $\text{Si}_3\text{N}_4$  powders. The distributions of Al and Ti determined using EDX, as shown in Fig. 2(a-2), were homogeneous. The phase of the  $\text{Si}_3\text{N}_4$  was identified as  $\beta$ -type  $\text{Si}_3\text{N}_4$  (P63,  $a = b = 7.595$  \AA,  $c = 2.902$

\AA), as shown in Fig. S1. The XPS depth analysis results shown in Fig. 2(b) reveal that the deposited layer was a multi-layered structure comprising Ti, Al, and a thin Al oxide layer from the  $\text{Si}_3\text{N}_4$  substrate to the surface. The thicknesses of the Ti, Al, and Al oxide layers were approximately 340, 174, and 7 nm, respectively. Thus, a multi-layered deposition layer was fabricated via serial Ti/Al deposition and subsequent air exposure after the deposition process.

Next, the bonding interface of the fabricated Cu/ $\text{Si}_3\text{N}_4$ /Cu substrate was analyzed. From the SAT observation of the bonding area shown in Fig. 3(a), Cu was well-bonded to the  $\text{Si}_3\text{N}_4$  substrate, and no apparent voids or delamination were observed. This is supported by the cross-sectional SEM image shown in Fig. 3(b), where an intermediate layer with a thickness of approximately 300 nm can be observed at the interface between Cu and  $\text{Si}_3\text{N}_4$ . The variation observed between the thickness of the initially sputtered Ti/Al bilayer and that of the intermediate layer could potentially stem from inaccuracies in the sputtering rate used in XPS.

The fabricated Cu/ $\text{Si}_3\text{N}_4$ /Cu substrate, as shown in Fig. 3(b), was further analyzed using TEM to understand the intermediate layer between the Cu and  $\text{Si}_3\text{N}_4$  substrates. Fig. 4 shows the TEM bright field (BF) image accompanied by EDX elemental mapping and line analysis, detailing the bonding interface. The Cu and  $\text{Si}_3\text{N}_4$  interface, as shown in Fig. 4(a), exhibited a 300 nm thick intermediate layer. The elemental maps in Fig. 4(b) show distinct Ti- and Al-rich regions interspersed within the intermediate layer. The line analysis results in Fig. 4(c) indicate that the intermediate layer is divided into Ti- and Al-rich regions. As previously highlighted, the layers initially deposited on the  $\text{Si}_3\text{N}_4$  substrate prior to bonding constituted a  $\text{Si}_3\text{N}_4$ /Ti/Al multi-layered configuration (refer to Fig. 2). However, after bonding, the intermediate layer exhibited segregated Ti- and Al-rich regions. An isolated island-like morphology of the Al-rich regions was observed, whereas the Ti-rich regions were partly isolated from each other. Despite the initial  $\text{Si}_3\text{N}_4$ /Ti/Al layer configuration before bonding, the Al-rich regions exhibited a tendency to adhere to the  $\text{Si}_3\text{N}_4$  surface.

Furthermore, TEM analysis was conducted on the intermediate layer, as shown in Fig. 5. The BF image and corresponding EDX maps shown in Fig. 5(a-f) reveal that Ti and N are attached adjacent to the Cu side, whereas Al and Cu tend to appear on the  $\text{Si}_3\text{N}_4$  side. Region 1, adjacent to the Cu side (see Fig. 5(a)), was indexed as TiN ( $\text{Fm}\bar{3}\text{m}$ ,  $a = 4.241$  \AA) based on the selected area diffraction pattern (SADP) and dark-field (DF)

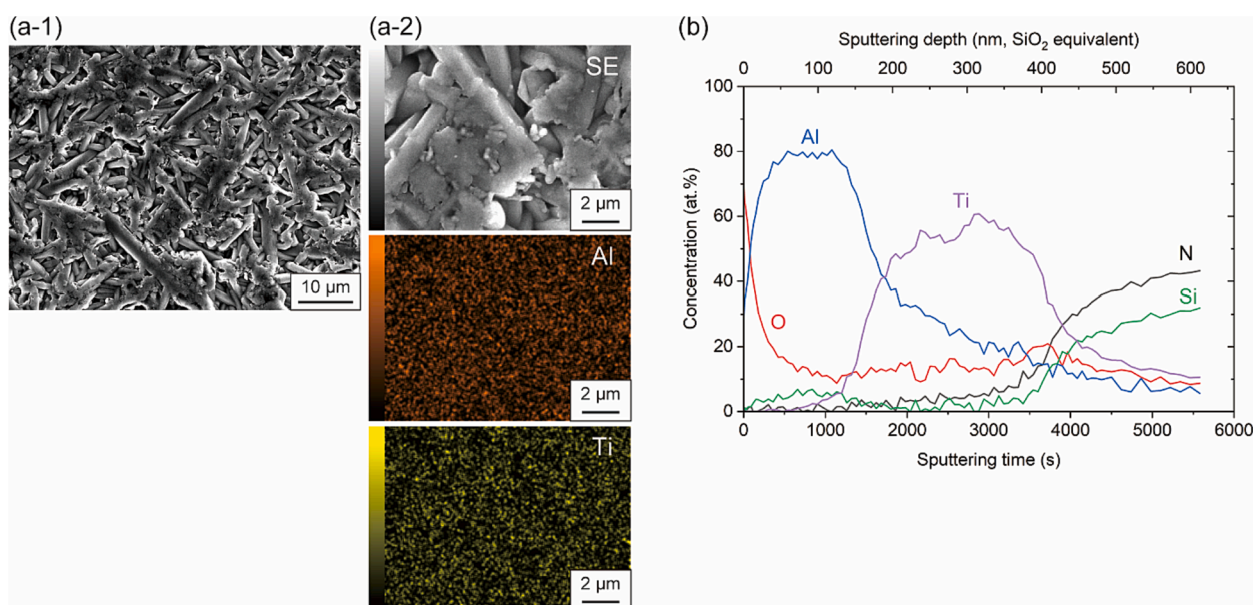
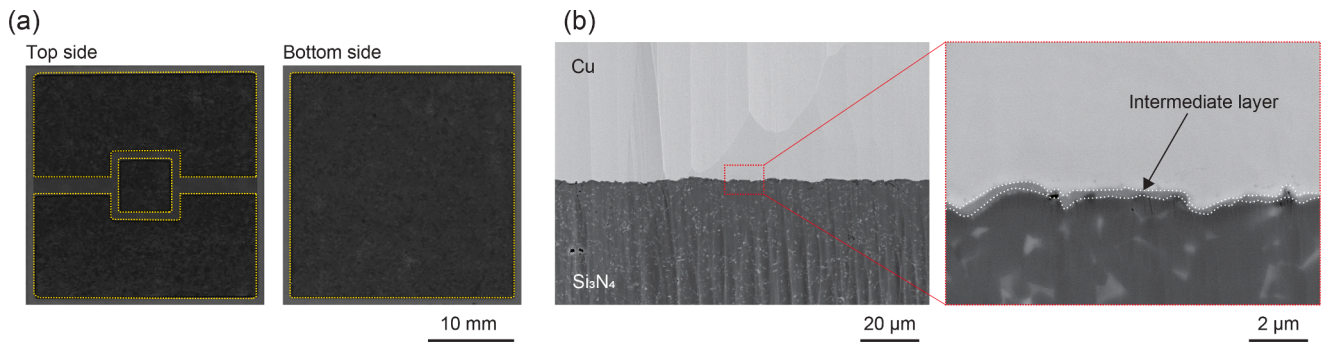


Fig. 2. Surface analysis results of the as-deposited  $\text{Si}_3\text{N}_4$  substrate: (a-1) SEM image and (a-2) EDX results of the as-deposited surface. (b) XPS depth analysis of its surface.



**Fig. 3.** Images of the fabricated Cu/Si<sub>3</sub>N<sub>4</sub>/Cu substrate: (a) SAT images from both top and bottom sides, with the bonding area outlined by yellow lines (in the SAT image, the bonded areas appear black, whereas the unbonded areas are white). (b) Cross-sectional SEM images at the Cu/Si<sub>3</sub>N<sub>4</sub> interface.

**Table 1**  
Summary of mechanical properties for materials used in this study [23–25].

Material	Young's modulus <i>E</i> (GPa)	Yield strength $\sigma_Y$ (MPa)	Ultimate tensile strength $\sigma_{UTS}$ (MPa)	CTE $\alpha$ (10 <sup>-6</sup> /K)	Poisson's ratio $\nu$ (-)
Si <sub>3</sub> N <sub>4</sub>	290	–	–	2.9	0.27
Cu	100 (0 °C)	52.4 (0 °C)	242 (0 °C)	16.7	0.33
	88 (300 °C)	42.3 (300 °C)	178 (300 °C)		

image, as shown in Fig. 5(g). Region 2, adjacent to the Si<sub>3</sub>N<sub>4</sub> side (see in Fig. 5(a)), was indexed as Cu<sub>9</sub>Al<sub>4</sub> (P43m, a = 8.703 Å) based on Fig. 5(h). Region 3, within Si<sub>3</sub>N<sub>4</sub> (see in Fig. 5(a)), was indexed as β-Si<sub>3</sub>N<sub>4</sub> (P6<sub>3</sub>, a = b = 7.632 Å, c = 2.920 Å) based on Fig. 5(i). Cu<sub>9</sub>Al<sub>4</sub> and β-Si<sub>3</sub>N<sub>4</sub> existed next to each other, even though they were partially overlapped by the FIB processing, suggesting their good affinity. The high-resolution

TEM (HRTEM) image of the interface between β-Si<sub>3</sub>N<sub>4</sub> and Cu<sub>9</sub>Al<sub>4</sub>, as shown in Fig. 5(j), supported their good lattice match, with corresponding lattice spacings of (110)<sub>β-Si<sub>3</sub>N<sub>4</sub></sub> and (210)<sub>Cu<sub>9</sub>Al<sub>4</sub></sub> at 3.82 and 3.88 Å, respectively.

### 3.2. Bonding behavior

Focusing on the interface between Si<sub>3</sub>N<sub>4</sub> and Ti, possible reactions between Si<sub>3</sub>N<sub>4</sub> and Ti have been proposed. Shimoo et al. [27] reported that heating a powder mixture of Si<sub>3</sub>N<sub>4</sub> and Ti in an Ar atmosphere to 1050 °C produced Ti<sub>2</sub>N, TiN, and Ti<sub>5</sub>Si<sub>3</sub>. In addition, they assumed the following reactions partly supported by the standard free energies of formation ( $\Delta G^0$ ):

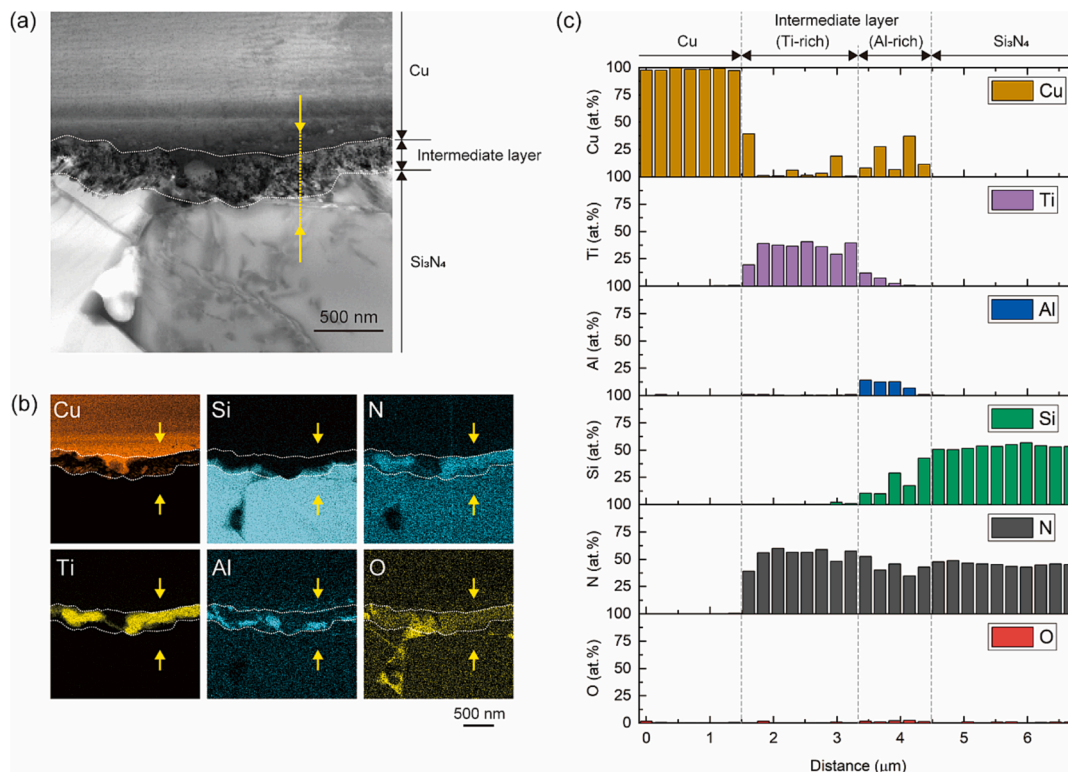
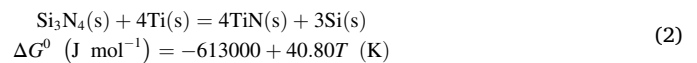
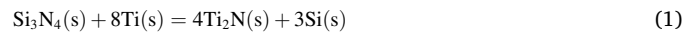


**Fig. 4.** TEM observation results of the Cu/Si<sub>3</sub>N<sub>4</sub> interface: (a) BF image, (b) EDX mapping, and (c) line analysis results. Yellow arrows indicate the location of the line analysis in (a) and (b).

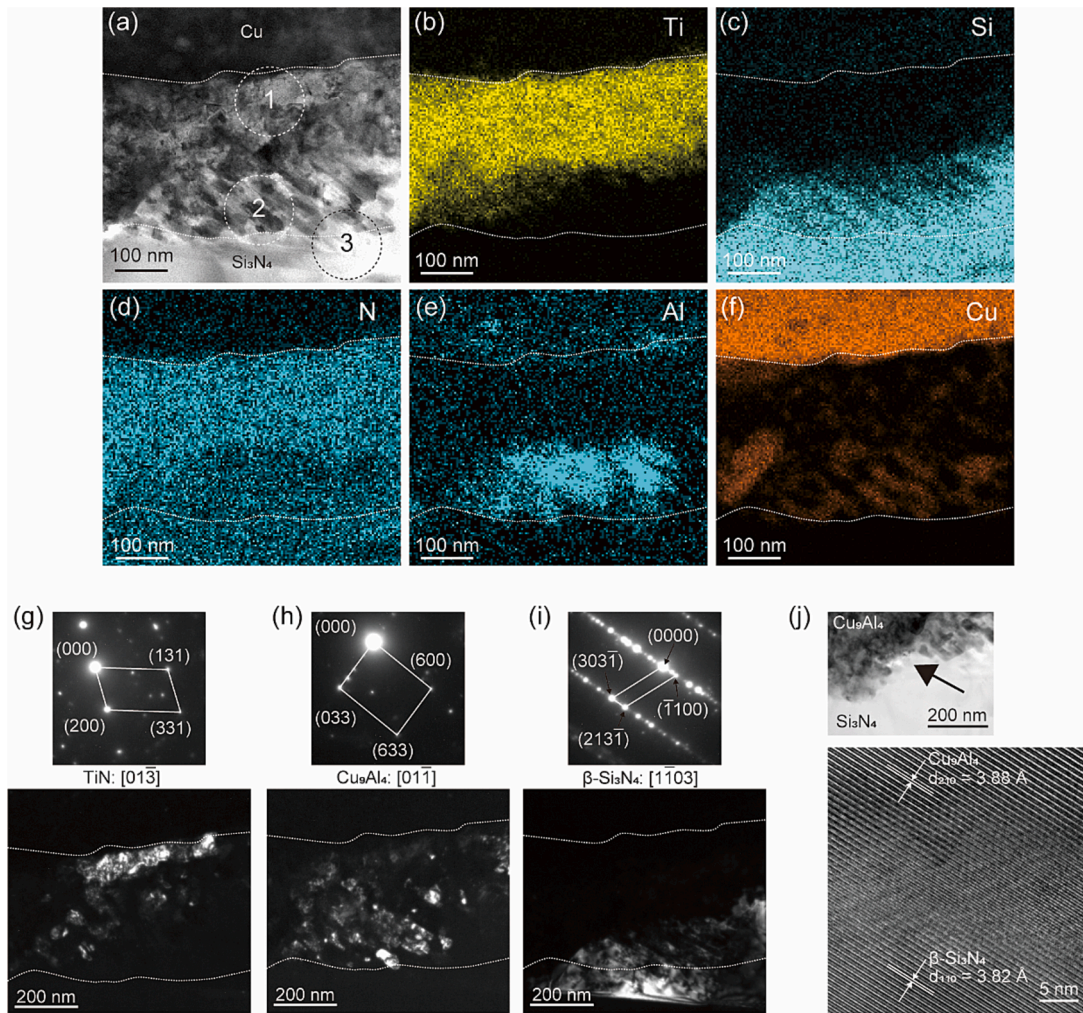
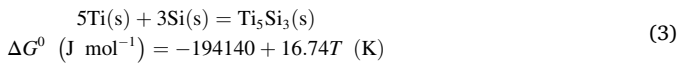


**Fig. 5.** TEM results of the intermediate layer: (a) BF image; EDX mappings of (b) Ti, (c) Si, (d) N, (e) Al, and (f) Cu. SADPs and DF images of (g) TiN, (h) Cu<sub>9</sub>Al<sub>4</sub>, and (i) β-Si<sub>3</sub>N<sub>4</sub>, corresponding to regions 1–3 in (a). (j) HRTEM image showing the interface between β-Si<sub>3</sub>N<sub>4</sub> and Cu<sub>9</sub>Al<sub>4</sub>.



Although information in the thermodynamic databases is limited [28–31], at least the reactions described in Eqs. (2) and (3) are likely to occur because  $\Delta G^0$  is negative. Based on Eqs. (1) and (2), Ti<sub>2</sub>N, TiN, and Si were formed during the reactions of Si<sub>3</sub>N<sub>4</sub> with Ti. Subsequently, the formed Si may react immediately with Ti to form Ti<sub>5</sub>Si<sub>3</sub>, according to Eq. (3). An experimental result was reported by Paulasto et al. [32], where the diffusion couple of Ti/Si<sub>3</sub>N<sub>4</sub> after aging at 950 °C for 24 h suggested a Ti/Ti<sub>5</sub>Si<sub>3</sub>/TiN/Si<sub>3</sub>N<sub>4</sub> interfacial structure. Ti<sub>2</sub>N was barely detectable, owing to its transformation into TiN. Using thermodynamic simulations, Ma et al. [33] predicted the interfacial structure of Ti/Ti<sub>5</sub>Si<sub>3</sub>N<sub>x</sub>/TiN/Si<sub>3</sub>N<sub>4</sub> for a Ti/Si<sub>3</sub>N<sub>4</sub> joint based on the calculation of phase diagram (CALPHAD) method. These studies suggest the formation of TiN and Ti<sub>5</sub>Si<sub>3</sub>N<sub>x</sub> at the Ti/Si<sub>3</sub>N<sub>4</sub> interface. In this study, TiN was detected at the bonding interface, whereas Ti<sub>5</sub>Si<sub>3</sub>N<sub>x</sub> was not. This may be because a small amount of Ti layer was immediately consumed. Based on this, Si may dissolve in molten Al, as described below. The preferential reaction of Ti with Si<sub>3</sub>N<sub>4</sub> over Al observed in this study remains not fully elucidated, attributed to the constraints of the available thermodynamic data. However, this preference may be due to  $\Delta G^0$  for the reactions depicted in Eqs. (1)–(3) being lower than that for the Ti–Al reaction.

The bonding behavior was presumed, as shown in Fig. 6. First, the Ti/Al layers deposited on the Si<sub>3</sub>N<sub>4</sub> faced the Cu surface prior to

bonding, as shown in Fig. 6(a). After heating, the deposited Ti layer reacted with Si<sub>3</sub>N<sub>4</sub> to form TiN and Si particles (Eq. (2)), as shown in Fig. 6(b). Next, upon heating to the melting point of Al (660 °C), the thin Al oxide layer fractured owing to the bonding pressure, followed by molten Al wetting on both the Cu and Ti surfaces, as shown in Fig. 6(c). During this process, molten Al filled the gaps at the bonding interface. Simultaneously, adjacent solid phases dissolved into the molten Al, as shown in Fig. 6(c). According to the binary phase diagram, the solubilities of Cu and Si in molten Al are significantly greater than that of Ti, with approximately 63 and 20 mass% for Cu and Si, respectively, and less than 1 mass% for Ti at 700 °C. Consequently, Cu and Si were readily dissolved in the molten Al, accompanied by Al penetration toward the Si<sub>3</sub>N<sub>4</sub> side, as shown in Fig. 6(d). Subsequently, during the Al solidification process, an intermediate layer with segregated Ti- and Al-rich phases formed, as shown in Fig. 6(e). Notably, the Al- and Ti-rich phases tended to be adjacent to the Si<sub>3</sub>N<sub>4</sub> and Cu sides, respectively (Fig. 4). This arrangement may result from the progression of the entire system in an energetically stable direction. Further investigation into the interfacial energies between these constituent materials would be intriguing.

### 3.3. Thermal cycling reliability

Thermal cycling reliability of the fabricated Cu/Si<sub>3</sub>N<sub>4</sub>/Cu substrate was assessed using TCT in the temperature range from –40 and 200 °C, as shown in Fig. 7. Fig. 7(a) shows the evolution of the delamination

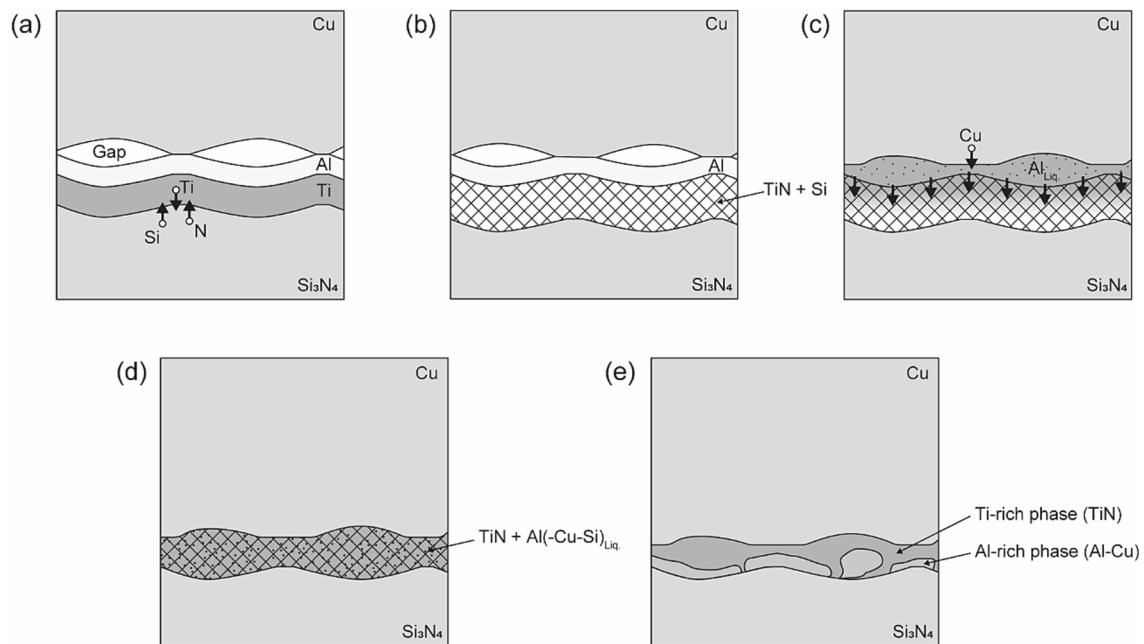


**Fig. 6.** Schematic showing the formation of the intermediate layer morphology with the segregated Ti- and Al-rich regions: (a) initial configuration at the bonding interface, (b) reaction between the deposited Ti layer and  $\text{Si}_3\text{N}_4$  substrate according to Eq. (2), (c) Al-layer melting at  $660\text{ }^\circ\text{C}$ , (d) dissolution of Cu and Si into molten Al and its penetration toward the  $\text{Si}_3\text{N}_4$  side, and (e) final product at the interface.

area ratio on the top and bottom sides during thermal cycling up to 600 cycles. The delamination area ratio on the top side increased with an increasing number of thermal cycles, reaching values of 7.0 %, 11.1 %, 19.5 %, and 27.3 % at 100, 200, 400, and 600 cycles, respectively. However, the values hardly increased on the bottom side, reaching 1.5 %, 1.8 %, 2.1 %, and 2.9 % at 100, 200, 400, and 600 cycles, respectively. The delamination area evolution on the top side was more obvious than that on the bottom side. The SAT images at 0, 200, and 600 cycles, as shown in Fig. 7(b), indicate that delamination occurred from the edges on the top side, but extremely little on the bottom side. The cross-sectional SEM image of the delaminated region on the top side (Fig. 7(c)) indicates that delamination occurred at the bonding interface.

The delamination behavior during the TCT was dominated by the cyclic thermal strain owing to the CTE mismatch between Cu and  $\text{Si}_3\text{N}_4$ . In this study, a mechanical FE simulation was performed to investigate the stress and strain distributions during TCT. A 3D 1/2 model, considering symmetry, was constructed by incorporating  $\text{Si}_3\text{N}_4$  and Cu layers, as shown in Fig. 7(d). The warpage trends during simulations at  $-40\text{ }^\circ\text{C}$  (cold side) and  $200\text{ }^\circ\text{C}$  (hot side) are shown in Fig. 7(e). The substrate warped upward by approximately 0.1 mm at  $-40\text{ }^\circ\text{C}$  but downward at  $200\text{ }^\circ\text{C}$ . This warpage behavior was influenced by the asymmetry between the top and bottom Cu patterns. To examine the tensile stress at the bonding interface, which may cause delamination, Fig. 7(f) illustrates the relationship between the maximum tensile stress in the top and bottom Cu layers and the number of thermal cycles. The top and bottom layers exhibit similar trends in response to thermal cycling. High maximum tensile stresses can be observed at the edges of the bonding area during the cold steps. Notably, the maximum tensile stress on the top side exceeds that on the bottom side. Furthermore, the peaks of the maximum tensile stresses at every cold step gradually increased with an increasing number of cycles owing to strain hardening. This is evidenced by the accumulated plastic strain against the thermal cycles, as shown in Fig. 7(g). The accumulated plastic strain increases linearly with the number of thermal cycles. The value of the top Cu layer is larger than that of the bottom layer. The larger accumulated plastic strain caused a higher tensile stress owing to strain hardening, which may have led to a larger delamination area on the top

side than on the bottom side.

Several studies have described the fracture behavior of traditional Cu–ceramic substrates during the TCT. They reported that cracks initiated at the corner edges of the Cu layers and propagated toward within ceramics of  $\text{Al}_2\text{O}_3$  [34,35], AlN [36], and  $\text{Si}_3\text{N}_4$  [8,36]. Furthermore, Pietranico et al. [37] numerically investigated TCT reliability on a DBC substrate, which indicated that the stress and strain fields were singular in the vicinity of the upper Cu layer edges, leading to crack initiation. The cracks observed in this study agree well with the knowledge of crack initiation sites in the literature. In contrast, the crack propagation route at the bonding interface in this study did not correspond to those inside the ceramics reported in the literature. The propagation route of cracks at the bonding interface or within the  $\text{Si}_3\text{N}_4$  substrate may depend on the disparity in their mechanical strengths.

#### 4. Conclusion

In this study, we propose a novel quasi-direct bonding technique that utilizes a Ti/Al active metal layer. A bonding interface without visible voids or delamination was achieved by prefabricating a sputtered Ti/Al bilayer on a  $\text{Si}_3\text{N}_4$  surface, followed by heating and pressing in vacuum. The melting of the Al layer, the subsequent dissolution/penetration phenomenon, and the chemical reaction of the Ti layer with  $\text{Si}_3\text{N}_4$  during the bonding process afforded a 300 nm thick intermediate layer comprising segregated Ti- and Al-rich phases with good lattice matching with  $\text{Si}_3\text{N}_4$ . Temperature cycling tests of the fabricated Cu/ $\text{Si}_3\text{N}_4$ /Cu substrates revealed a tendency toward delamination from both experimental and numerical points of view. The delamination was attributed to increased tensile stresses owing to strain hardening at the edges of the joints resulting from the asymmetric Cu pattern on the substrate. To verify the reliability of this bonding technique against a conventional AMB method, it would be required to fabricate and compare substrates involving Cu patterns with a consistent geometry.

Notably, these findings reveal that this innovative quasi-direct Cu– $\text{Si}_3\text{N}_4$  bonding technique holds great potential for solving the issues of electrochemical migration and void formation associated with Ag-containing brazing filler metals on AMB substrates. To further improve the thermal cycling reliability, mitigating the asymmetry of the

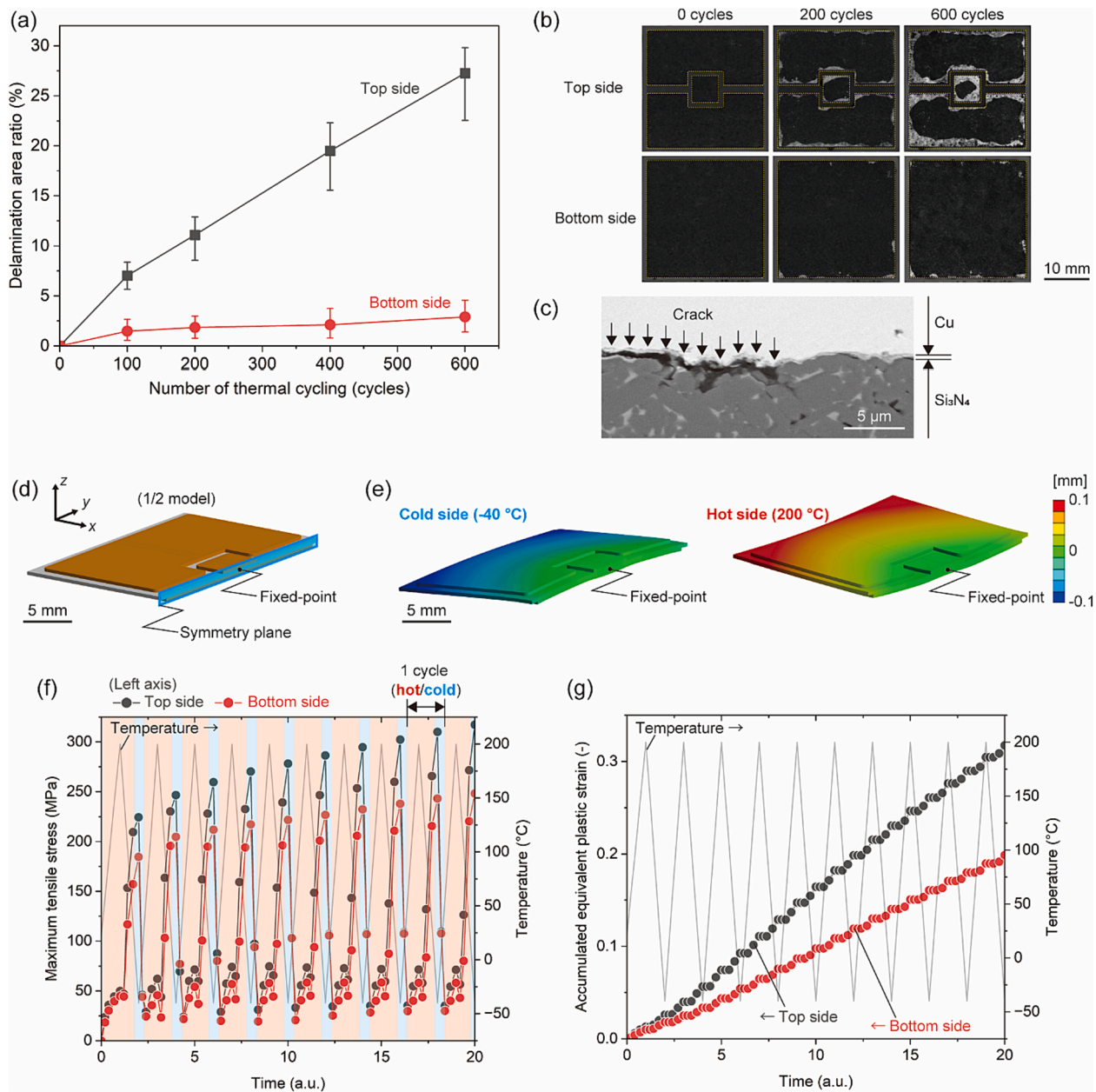


**Fig. 7.** TCT result of fabricated Cu/Si<sub>3</sub>N<sub>4</sub>/Cu substrate and FE simulation results: (a) Evolution of delamination area ratio on the top and bottom sides against thermal cycling in the temperature range from -40 to 200 °C. (b) SAT images of the top and bottom sides during thermal cycling of 0, 200, and 600 cycles. (c) Cross-sectional SEM image of crack at the bonding interface. (d) 1/2 symmetrical FE simulation model of Cu/Si<sub>3</sub>N<sub>4</sub>/Cu substrate. (e) Warpage at cold (-40 °C) and hot side (200 °C). (f) Maximum tensile stress on the top and bottom Cu layers during thermal cycles, where red and blue regions present high and low temperature steps, respectively. (g) Accumulated equivalent plastic strain on the top and bottom Cu layers during thermal cycles.

top and bottom Cu patterns and alleviating the stress concentration at the edge of the bonding region (e.g., by controlling the local shapes of the pattern edges during etching) would be of particular interest. Additionally, further optimization of the structure of the sputtered layers is anticipated. This study provides important insights into the Cu/Si<sub>3</sub>N<sub>4</sub> interface structure and facilitates advancements in bonding technology tailored to the future of power electronics.

#### CRediT authorship contribution statement

**Hiroaki Tatsumi:** Conceptualization, Methodology, Validation, Investigation, Writing – original draft, Visualization. **Seongjae Moon:** Investigation, Methodology. **Makoto Takahashi:** Investigation. **Takahiro Kozawa:** Investigation, Visualization, Writing – review & editing.

**Eiki Tsushima:** Funding acquisition, Investigation. **Hiroshi Nishikawa:** Supervision, Writing – review & editing.

#### Declaration of competing interest

The authors declare that they have no known competing financial interests or personal relationships that could have appeared to influence the work reported in this paper.

#### Data availability

Data will be made available on request.



## Acknowledgement

This work was partially supported by the Go-Tech Project of the Hokkaido Bureau of Economy, Trade, and Industry.

## Appendix A. Supplementary data

Supplementary data to this article can be found online at <https://doi.org/10.1016/j.matdes.2024.112637>.

## References

- J.G. Kassakian, T.M. Jahns, Evolving and emerging applications of power electronics in systems, *IEEE J. Emerg. Sel. Top. Power Electron.* 1 (2013) 47–58.
- M.M. Tousi, M. Ghassemi, Characterization of nonlinear field-dependent conductivity layer coupled with protruding substrate to address high electric field issue within high-voltage high-density wide bandgap power modules, *IEEE J. Emerg. Sel. Top. Power Electron.* 8 (2020) 343–350.
- Y. Wang, Y. Ding, Z. Yuan, H. Peng, J. Wu, Y. Yin, T. Han, F. Luo, Space-charge accumulation and its impact on high-voltage power module partial discharge under DC and PWM waves: testing and modeling, *IEEE Trans. Power Electron.* 36 (2021) 11097–11108.
- G. Mirone, A. Sitta, G. D'Arrigo, M. Calabretta, Material characterization and warpage modeling for power devices active metal brazed substrates, *IEEE Trans. Device Mater. Reliab.* 19 (2019) 537–542.
- E. Gurpinar, B. Ozpıneci, S. Chowdhury, Design, analysis, comparison, and experimental validation of insulated metal substrates for high-power wide-bandgap power modules, *J. Electron. Packag.* 142 (2020) 041107.
- H. Lee, V. Smet, R. Tummala, A review of SiC power module packaging technologies: challenges, advances, and emerging issues, *IEEE J. Emerg. Sel. Top. Power Electron.* 8 (2020) 239–255.
- L. Xu, M. Wang, Y. Zhou, Z. Qian, S. Liu, An optimal structural design to improve the reliability of Al<sub>2</sub>O<sub>3</sub>-DBC substrates under thermal cycling, *Microelectron. Reliab.* 56 (2016) 101–108.
- D.P. Hamilton, S. Riches, M. Meisser, L. Mills, P. Mawby, High temperature thermal cycling performance of DBA, AMB and thick film power module substrates, in: CIPS 2016; 9th International Conference on Integrated Power Electronics Systems, *ieeexplore.ieee.org*, 2016: pp. 1–5.
- D. Kim, Y. Yamamoto, S. Nagao, N. Wakasugi, C. Chen, K. Suganuma, Measurement of heat dissipation and thermal-stability of power modules on DBC substrates with various ceramics by SiC micro-heater chip system and Ag sinter joining, *Micromachines (Basel)* 10 (2019), <https://doi.org/10.3390/mi10110745>.
- H.M. Lee, E.B. Lee, D.L. Kim, D.K. Kim, Comparative study of oxide and non-oxide additives in high thermal conductive and high strength Si<sub>3</sub>N<sub>4</sub> ceramics, *Ceram. Int.* 42 (2016) 17466–17471.
- T. Lu, T. Wang, Y. Jia, M. Ding, Y. Shi, J. Xie, F. Lei, L. Zhang, L. Fan, Fabrication of high thermal conductivity silicon nitride ceramics by pressureless sintering with MgO and Y<sub>2</sub>O<sub>3</sub> as sintering additives, *Ceram. Int.* 46 (2020) 27175–27183.
- A. Fukumoto, D. Berry, K.D.T. Ngo, G.-Q. Lu, Effects of extreme temperature swings (−55°C to 250°C) on silicon nitride active metal brazing substrates, *IEEE Trans. Device Mater. Reliab.* 14 (2014) 751–756.
- G. Böhm, D. Brunner, I. Sichert, A. Pönicke, J. Schilm, Properties and reliability of Silicon Nitride substrates with AMB copper conductor, *IMAPS - International Microelectronics Assembly and Packaging Society* (2011) 000777–000784.
- Y. Mori, S. Fujisawa, K. Morimoto, M. Yonei, H. Kato, S. Suenaga, Development of Ag-free active metal brazing filler for manufacturing copper-Si<sub>3</sub>N<sub>4</sub> substrates, in: *PCIM Europe 2023; International Exhibition and Conference for Power Electronics, Intelligent Motion, Renewable Energy and Energy Management*, *ieeexplore.ieee.org*, 2023: pp. 1–6.
- G.T. Kohman, H.W. Hermance, G.H. Downes, Silver migration in electrical insulation, *Bell Syst. Tech. J.* 34 (1955) 1115–1147.
- S. Yang, J. Wu, A. Christou, Initial stage of silver electrochemical migration degradation, *Microelectron. Reliab.* 46 (2006) 1915–1921.
- N.F. Kazakov, *Diffusion Bonding of Materials*, Elsevier, 2013.
- J. Schulz-Harder, Advantages and new development of direct bonded copper substrates, *Microelectron. Reliab.* 43 (2003) 359–365.
- Y. Song, H. Zhu, D. Liu, X. Song, C. Tan, J. Cao, Direct bonding of silicon nitride to copper via laser surface modification, *Appl. Surf. Sci.* 602 (2022) 154354.
- Y. Song, D. Liu, G. Jin, H. Zhu, N. Chen, S. Hu, X. Song, J. Cao, Fabrication of Si<sub>3</sub>N<sub>4</sub>/Cu direct-bonded heterogeneous interface assisted by laser irradiation, *J. Mater. Sci. Technol.* 99 (2022) 169–177.
- G. Liu, D. Wang, Y. Xing, X. Zhong, W. Pan, Copper bonding silicon nitride substrate using atmosphere plasma spray, *J. Eur. Ceram. Soc.* 43 (2023) 3981–3987.
- C. Xin, R. Yuan, J. Wu, Q. Wang, Y. Zhou, Fabrication and joining mechanism of Nano-Cu/Si<sub>3</sub>N<sub>4</sub> ceramic substrates, *Ceram. Int.* 47 (2021) 3411–3420.
- C. Chen, C. Choe, Z. Zhang, D. Kim, K. Suganuma, Low-stress design of bonding structure and its thermal shock performance (−50 to 250 °C) in SiC/DBC power die-attached modules, *J. Mater. Sci. Mater. Electron.* 29 (2018) 14335–14346.
- W.D. Jenkins, T.G. Digges, C.R. Johnson, Tensile properties of copper, nickel, and 70% copper/30% nickel and 30% copper/70% nickel alloys at high temperatures, *J. Res. Nat. Bur. Stand.* 58 (1957) 201–211.
- H. Tatsumi, H. Yamaguchi, T. Matsuda, T. Sano, Y. Kashiba, A. Hirose, Deformation behavior of transient liquid-phase sintered Cu-solder-resin microstructure for die-attach, *Appl. Sci.* 9 (2019) 3476–3490.
- H. Miyazaki, Y. Zhou, S. Iwakiri, H. Hirotsuru, K. Hirao, S. Fukuda, N. Izu, H. Hyuga, Improved resistance to thermal fatigue of active metal brazing substrates for silicon carbide power modules using tough silicon nitrides with high thermal conductivity, *Ceram. Int.* 44 (2018) 8870–8876.
- T. Shimoo, K. Okamura, S. Adachi, Interaction of Si<sub>3</sub>N<sub>4</sub> with titanium at elevated temperatures, *J. Mater. Sci.* 32 (1997) 3031–3036.
- E.T. Turkdogan, *Physical chemistry of high temperature technology*, Academic Press, San Diego, CA, 1980.
- D.D. Wagman, W.H. Evans, V.B. Parker, Erratum: the NBS tables of chemical thermodynamic properties. Selected values for inorganic and C1 and C2 organic substances in SI units, *J. Phys. Chem.* (1989). <https://pubs.aip.org/aip/jpr/article-abstract/18/4/1807/241462>.
- P. Linstrom, NIST Chemistry WebBook, NIST Standard Reference Database 69, (1997). <https://doi.org/10.18434/T4D303>.
- T.C. Allison, NIST-JANAF Thermochemical Tables – SRD 13 (2013). <https://doi.org/10.18434/T42S31>.
- M. Paulasto, J.K. Kivilahti, F.J.J. van Loo, Interfacial reactions in Ti/Si<sub>3</sub>N<sub>4</sub> and TiN/Si diffusion couples, *J. Appl. Phys.* 77 (1995) 4412–4416.
- X. Ma, C. Li, W. Zhang, The thermodynamic assessment of the Ti–Si–N system and the interfacial reaction analysis, *J. Alloy. Compd.* 394 (2005) 138–147.
- L. Xu, S. Liu, M. Wang, S. Zhou, Crack initiation and propagation mechanism of Al<sub>2</sub>O<sub>3</sub>-DBC substrate during thermal cycling test, *Eng. Fail. Anal.* 116 (2020) 104720.
- P. Gaiser, M. Klingler, J. Wilde, The influence of strain hardening of copper on the crack path in Cu/Al<sub>2</sub>O<sub>3</sub>/Cu direct bonded copper substrates, *Int. J. Fatigue* 140 (2020) 105821.
- H. Miyazaki, S. Iwakiri, K. Hirao, S. Fukuda, N. Izu, Y.-I. Yoshizawa, H. Hyuga, Effect of high temperature cycling on both crack formation in ceramics and delamination of copper layers in silicon nitride active metal brazing substrates, *Ceram. Int.* 43 (2017) 5080–5088.
- S. Pietranico, S. Pommier, S. Lefebvre, Z. Khatir, S. Bontemps, Characterisation of power modules ceramic substrates for reliability aspects, *Microelectron. Reliab.* 49 (2009) 1260–1266.